Design and Validation of an Image-Guided Robot for Small Animal Research

Peter Kazanzides[1], Jenghwa Chang[3], Iulian Iordachita[1], Jack Li[2], C. Clifton Ling[3], and Gabor Fichtinger[1]

[1] Department of Computer Science, Johns Hopkins University, USA
pkaz@jhu.edu
[2] Department of Mechanical Engineering, Johns Hopkins University, USA
[3] Medical Physics Department, Memorial Sloan Kettering Cancer Center, USA*

Abstract. We developed an image-guided robot system to achieve highly accurate placement of thin needles and probes into in-vivo rodent tumor tissue in a predefined pattern that is specified on a preoperative image. This system can be used for many experimental procedures where the goal is to correlate a set of physical measurements with a corresponding set of image intensities or, more generally, to perform a physical action at a set of anatomic points identified on a preoperative image. This paper focuses on the design and validation of the robot system, where the first application is to insert oxygen measurement probes in a three-dimensional (3D) grid pattern defined with respect to a PET scan of a tumor. The design is compatible with CT and MRI, which we plan to use to identify targets for biopsy and for the injection of adenoviral sequences for gene therapy. The validation is performed using a phantom and includes a new method for estimating the Fiducial Localization Error (FLE) based on the measured Fiducial Distance Error (FDE).

1 Introduction

We are investigating non-invasive methods for identifying hypoxic (oxygen deficient) cells in tumors. This is important because hypoxic cells are resistant to radiation treatment and therefore treatment can be improved by tailoring the radiation dosage directed at them. By measuring the tissue oxygen tension (pO_2) level of the cells using an Oxylite probe[1] and correlating these measurements with Positron Emission Tomography (PET) scan data, it is possible to verify the efficacy of PET scans for locating hypoxic cancer cells prior to radiation treatment[2]. Initially, we used a manual method to verify the correlation between PET scan data and pO_2 measurements for tumors on rodents. The procedure was to place the anesthetized rodent inside a foam-filled bed that contained a template with PET-compatible markers. After the PET scans, the entire rodent and bed assembly were placed beneath a passive fixture that held

* We thank Emese Balogh, Anton Deguet, Russell Taylor (JHU), Bixiu Wen, Pat Zanzonico, Andrei Pugachev, Qing Chen, Jose Campa (MSKCC) for their assistance. This work is supported by NIH RO1 CA84596 and NSF EEC 9731748.

R. Larsen, M. Nielsen, and J. Sporring (Eds.): MICCAI 2006, LNCS 4190, pp. 50–57, 2006.

the Oxylite probe. A set of measurement targets (a "track") on the PET image was selected and the corresponding template hole was located. After the skin and tumor were punctured with a needle, the Oxylite probe was manually advanced through the template hole to measure the pO_2 level at each point along the track. This procedure was repeated for multiple template holes (tracks). Our goal was to design and build a robot system to automate this time-consuming and labor-intensive procedure, while eliminating the constraint that measurement tracks be defined only through template holes. The desired accuracy of the robot system was specified to be 0.25 mm or better, not including the error due to the imaging system.

2 System Design

2.1 Hardware Design

The robot system consists of a mobile cart that houses the electronics and provides a table top for the four axis robot and display (see Fig. 1). The robot is composed of a two degree-of-freedom X-Y horizontal platform and two vertical slides (Z1, Z2). A horizontal arm is mounted on the first vertical slide (Z1) and provides an attachment for either a registration probe or cannula. The second vertical slide (Z2) is attached to the first vertical slide and contains a probe holder. This allows the system to insert the Oxylite probe through the cannula and into the tumor. Note that in this case, the Z1 axis positions the cannula near the skin surface and the Z2 axis drives the measurement probe to the target.

The rodent bed (Fig. 2) fits inside the limited bore of the small animal imaging scanners and mounts onto the robot X-Y platform. It includes markers for the registration between image and robot coordinates. The markers are mounted on an adjustable bridge so that they can be positioned over the target region (tumor) and within the scanner field of view. The bridge is removed after registration to enable access to the rodent. As shown in Fig. 2, we initially used the Acustar® marker system[3], donated by Z-Kat Inc. (Hollywood, Florida, USA), for the CT, MRI and robot markers and a separate set of support tubes (offset by a known amount) for the radioactive PET markers. We are currently using a simpler marker system that consists of four small hemispheres (3 mm diameter), drilled into the adjustable bridge. These hemispheres are filled with an appropriate contrast agent prior to imaging. After imaging, the contrast agent is removed and the holes are physically located by the robot. For this procedure, the cannula is replaced by a registration probe, which is guided to the markers using a force control mode[4]. Force control is possible because the system contains a two-axis sensor (XY) beneath the rodent bed and a single-axis sensor (Z1) near the attachment mechanism for the registration probe and cannula.

The robot controller consists of a rackmount computer connected via Ethernet to a DMC-2143 controller board and AMP-20540 power amplifier (Galil Motion Control, Rocklin, CA, USA). The controller provides low-level servo control of the four robot motors. Application software on the PC sends position goals via Ethernet to the controller, which then moves each joint to its goal. The power

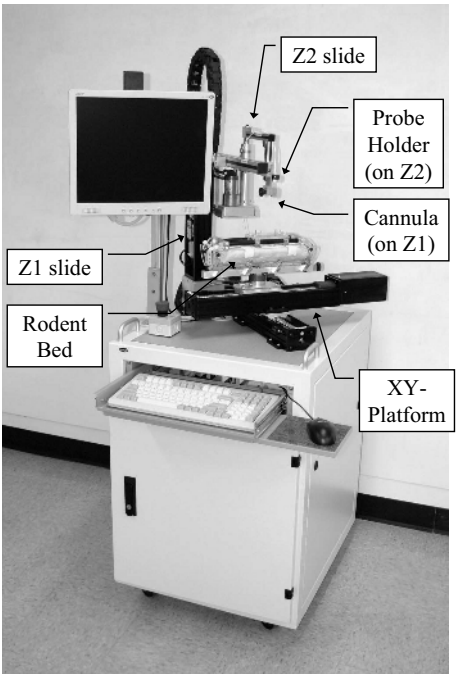

Fig. 1. Robot system

Fig. 2. Rodent bed with marker bridge

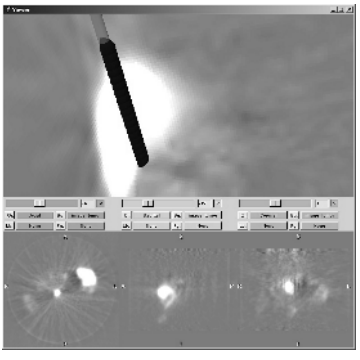

Fig. 3. Measurement track in PET

amplifier provides eight analog inputs, three of which are used for the interface to the force sensors. For the XY force sensor, we used the DX-480 from Bokam Engineering (Santa Ana, CA, USA) with a custom amplifier board that fits inside a shielded metal case below the sensor body. The Z1 force sensor is an L2357 sensor manufactured by Futek, Inc. (Irvine, CA, USA).

2.2 Software Design

We developed the application software, using 3D Slicer (www.slicer.org), to guide the user through most steps of the procedure, which are:

1. Place anesthetized tumor-bearing rodent in rodent bed.
2. Place rodent bed in scanner and obtain image data.
3. Move rodent bed to robot system and load image data into computer.
4. Register image data to robot:
   (a) Manually guide robot's registration probe into contact with each of the four markers.
   (b) Use a semi-automatic image processing procedure to locate the corresponding image markers.
   (c) Perform an optimization to determine the transformation that aligns the two sets of marker positions (robot and image).

5. Remove registration probe from Z1 axis and attach cannula.
6. Attach measurement (Oxylite) probe to Z2 axis and zero its position.
7. Identify target regions (sets of vertical tracks) in the image (see Fig. 3).
8. Transform the track points to robot coordinates and move the robot so that it positions the cannula at the entry point of the first probe track.
9. Prompt the user to manually puncture the skin by inserting a needle through the cannula and then removing it.
10. Command the robot to move the measurement probe through the cannula and into the tumor. The robot moves the probe vertically inside the tumor in user-defined increments (typically 1 mm), recording data at each position.
11. When the measurement probe reaches the end of the current track, command the robot to retract the probe back inside the cannula, move it to the starting point of the next track, and repeat the above cannula insertion and probe measurement sequence until the entire grid pattern has been traversed.

The manual guidance feature is achieved by a force control algorithm that uses nonlinear gains to provide fine positioning without sacrificing maximum motion speed[4]. A simplified representation of the nonlinear force control equation is given by:

$$V_i = F_i * G_i * (1 - \cos(9 * F_i))$$

where V_i, F_i and G_i are the commanded velocity, measured force and maximum admittance gain for axis i, respectively. The multiplication by 9 ensures that the maximum force reading (10 Volts) produces the largest commanded velocity because cos(90) is 0. The nonlinear factor $1 - \cos(9 * F_i)$ is relatively flat for low forces but has a higher slope for large forces. The actual implementation includes a deadband (so that sensor noise does not cause unwanted motion) and another nonlinear factor that is a function of the distance to the travel limit (so that the robot slows down as it approaches the limit).

The transformation ${}^R_I T$ between image coordinates and robot coordinates is obtained by performing a best-fit estimation between the two 3D point sets (4 image markers and 4 robot markers). There are several closed-form solutions that minimize a cost function that is the sum of the squared L2-norms, where ${}^R P_k$ and ${}^I P_k$, $k = 1 \ldots N$, are the robot and image marker positions, respectively ($N = 4$ in our case):

$$Cost = \sum_{k=1}^{N} \left|\left| {}^R P_k - {}^R_I T \; {}^I P_k \right|\right|^2 \tag{1}$$

Due to a somewhat arbitrary implementation decision, we instead compute an initial transformation using three of the markers and then iteratively estimate the final transformation using a variation of Powell's Method [5]. This minimizes a cost function as given in equation (1), except that the L2-norms are not squared. Although our method has the potential advantage of being less sensitive to outliers (because the errors are not squared), it has the disadvantage of being incompatible with much of the literature, which assumes the formulation

of equation (1). For example, the Fiducial Registration Error (FRE) is defined based on the minimum value of equation (1):

$$FRE = \sqrt{\frac{1}{N}\sum_{k=1}^{N} \left|\left|{}^{R}P_k - {}^{R}_{I}T_i \; {}^{I}P_k\right|\right|^2} \tag{2}$$

To avoid confusion, the results of the phantom experiments reported in the next section were computed (offline) using the standard technique described by Arun[6] and modified by Umeyama[7], instead of the iterative technique. In our testing, we noted minor differences between the registrations obtained with these two methods and we intend to replace the iterative technique with this closed-form technique.

3 Phantom Experiments

We performed several tests using a phantom to evaluate the accuracy of the overall system, as well as the accuracy of the major subsystem components (imaging system and robot). Following the terminology of [3], we focus on the following categories of error:

Fiducial localization error (FLE): error in determining the position of a marker in image coordinates (FLE-I) or robot coordinates (FLE-R).

Target registration error (TRE): mean error for locating markers that were not used for registration. This is most relevant to the application.

3.1 Phantom Design

We designed a phantom (Fig. 4) that has 20 small hemispherical holes (1-20), 2 cylindrical holes (C1-C2) and 4 large registration holes (R1-R4) arranged at 5 different heights. The 2 cylindrical holes and 4 large registration holes (R1-R4) were not used for any of the tests reported here and will not be discussed further. The 20 small holes have a diameter of 3 mm and are therefore equivalent to the markers on the rodent bed. Four of these holes (1, 3, 10, 11) are arranged in the same pattern as the four markers on the rodent bed. We chose Delrin because it is compatible with all image modalities of interest (PET, CT, MRI). The phantom is 120mm x 50mm x 45mm, which is small enough to fit inside all small animal scanners. It was machined on a CNC machine with a known accuracy of ± 0.0005 inches (± 0.0127mm). Considering the material properties of Delrin, we estimate the overall accuracy of the phantom to be ± 0.05mm. Because our "hole finding" procedure with the robot is a manual task involving hand-eye coordination, we darkened the edges of the holes to obtain sufficient visual contrast.

For microPET imaging of the phantom, the hemispherical holes were filled with contrast agent (radioactive tracer). After scanning, the application software was used to find the centroid of each marker in the image. For the robot measurements, the robot's registration probe was manually guided to each accessible hole. The data was analyzed to determine the Fiducial Localization Errors (FLE-I and FLE-R) and the Target Registration Error (TRE).

3.2 Fiducial Localization Error (FLE)

FLE can be simply defined as "the error of determining the positions of the markers" [3], but it can be difficult to measure directly. One approach is to infer FLE from FRE, using the following approximation (see [8]):

$$FLE = \sqrt{\left(\frac{N}{N-2}\right) FRE^2} \tag{3}$$

This is especially useful with an accurately-machined (CNC) phantom because it can be individually applied to each measurement subsystem (image and robot). Furthermore, the phantom can contain a large number of markers and thereby produce a robust estimate of FLE.

We developed an alternate method for estimating FLE based on the Fiducial Distance Error (FDE) which we define as the difference, for each pair of markers, between the measured distance and the known distance. For example, if P_{ab} is the measured distance between markers a and b (in image or robot coordinates) and C_{ab} is the distance between those markers in CNC coordinates, the FDE is $|P_{ab} - C_{ab}|$. Note that for N markers, there are a total of $N(N-1)/2$ measurements. The relationship between FLE (assumed identical at each marker) and the average FDE depends on the geometrical arrangement of the markers. We performed simulations to obtain an empirical relationship. Each simulated data set was created by adding zero-mean Gaussian noise, with a specified standard deviation (applied isotropically), to the CNC coordinates of each phantom marker. For each standard deviation, we created 10,000 simulated data sets and computed the average FDE. We performed separate simulations for the image markers and the robot markers because even though we used the same phantom, 14 markers were in the PET field of view and 16 markers were accessible by the robot. In both cases, we obtained a linear relationship between FLE and FDE, with the ratio FLE/FDE approximately equal to 1.5.

3.3 Target Registration Error (TRE)

It is first necessary to find the four registration markers in PET and robot coordinates and compute the transformation between these two coordinate systems. The TRE is then determined by transforming all other markers (not used for registration) into a common coordinate system and computing the distance between each set of corresponding points; for example, if P_5 and R_5 are the positions of point 5 in PET and robot coordinates, respectively, and ${}^R_I T$ is the transformation from PET (image) to robot coordinates, the TRE for point 5 is given by $\left|R_5 - {}^R_I T P_5\right|$.

TRE is the most meaningful measurement of the overall system accuracy because it estimates the accuracy with which the robot can position the instrument (Oxylite probe) at the location identified on the PET image. It is important, however, to understand the limitations of the test conditions. The phantom tests do

not include errors due to instrument compliance/bending or to the motion of the target (tumor). In the case of the fiber-optic Oxylite probe, the error due to bending can be significant. Furthermore, the TRE value does not include any error due to the tool drive axis (Z2).

4 Results

The hemispherical markers in the phantom were filled with 5 μl of ^{18}F-FDG (26.5 μCi). Only 14 markers (1-14) were visible in the microPET scanner's limited field of view. On the robot, it proved to be too difficult to see the 4 deepest markers (2, 7, 13, 17) and therefore they were eliminated from the testing.

4.1 PET Image Fiducial Localization Error (FLE-I)

One microPET scan of the phantom was acquired and the application software was used to find all 14 imaging markers (filled holes) in the field of view. We used a corrected value (1.229 mm) for the PET slice spacing that had been experimentally determined during earlier testing.

The 14 markers resulted in 91 computed distance errors and yielded an FDE-I of 0.172 $\pm$0.121 mm (mean $\pm$ standard deviation). The largest distance error was 0.497 mm. Our simulations produced the empirical relationship FLE-I = 1.49*FDE-I, which estimates FLE-I to be 0.26 mm.

For comparison, we applied the standard least-squares registration technique [6][7] to all 14 imaging markers. The resulting FRE was 0.236 mm, which according to equation (3), with $N = 14$, estimates FLE-I to be 0.26 mm.

4.2 Robot Fiducial Localization Error (FLE-R)

The robot was used to locate the 16 accessible markers in three different trials. Each trial yielded 120 computed distance errors, with an FDE-R value (over all three trials) of 0.121 $\pm$ 0.096 mm (mean $\pm$ standard deviation). The largest distance error was 0.455 mm. Our simulations produced the empirical relationship FLE-R = 1.51*FDE-R, which estimates FLE-R to be 0.18 mm.

Once again, we compared our result to the one obtained by applying equation (3) to the FRE from the least-squares registration of all 16 markers. For the data obtained from the three trials, the FRE was 0.168, 0.127, and 0.117 mm, for a mean value of 0.137 mm. This estimates FLE-R to be 0.15 mm.

4.3 Target Registration Error (TRE)

There were 11 markers, including all 4 reference markers, that were found in the PET image and by the robot. Therefore, it was possible to register the PET data set to each of the 3 robot data sets and compute TRE for the 7 target markers (see Table 1).

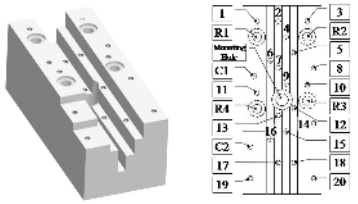

Fig. 4. Phantom

Table 1. Target Registration Error, mm

Trial	FRE	TRE		
		Mean	Std Dev	Max
1	0.217	0.305	0.098	0.447
2	0.200	0.293	0.088	0.395
3	0.227	0.279	0.105	0.475
Mean	0.215	0.292	0.097	

5 Conclusions

We completed the design of an image-guided robot system to assist with cancer research and performed phantom experiments to measure its accuracy. Our results indicate a mean positioning accuracy (TRE) of 0.29 mm, with the accuracy of the robot system alone well within the 0.25 mm specification. The results do not include errors due to the instrument drive unit (Z2 axis), instrument compliance/bending, or motion of the target (tumor). The largest error source is marker localization in the PET image (FLE-I), followed by marker localization by the robot (FLE-R). We introduced a new method for estimating FLE based on distance errors (FDE) and found good agreement with the existing method based on FRE. Our results indicate that this robot system should improve the efficiency and accuracy of needle-based procedures for in-vivo measurement, biopsy, and injection in small animals.

References

1. Urano, M., Chen, Y., Humm, J., Koutcher, J., Zanzonico, P., Ling, C.: Measurements of tumor tissue oxygen tension using a time-resolved luminescence-based optical oxylite probe: Comparison with a paired survival assay. Radiation Research **158** (2002) 167–173
2. Cherry, S., Shao, Y., et al.: MicroPET: A high resolution PET scanner for imaging small animals. IEEE Trans. on Nuclear Science **44** (1997) 1161–1166
3. Maurer, C., Fitzpatrick, J., Wang, M., Galloway, R., Maciunas, R., Allen, G.: Registration of head volume images using implantable fiducial markers. IEEE Trans. on Medical Imaging **16** (1997) 447–462
4. Kazanzides, P., Zuhars, J., Mittelstadt, B., Taylor, R.: Force sensing and control for a surgical robot. In: IEEE Intl. Conf. on Robotics and Automation, Nice, France (1992) 612–617
5. Press, W., Teukolsky, S., Vetterling, W., Flannery, B.: Numerical Recipes in C. 2 edn. Volume 1. Cambridge University Press, Cambridge, UK (1992)
6. Arun, K., Huang, T., Blostein, S.: Least-squares fitting of two 3-D point sets. IEEE Trans. on Pattern Analysis and Machine Intelligence **9** (1987) 698–700
7. Umeyama, S.: Least-squares estimation of transformation parameters between two point patterns. IEEE Trans. Pattern Anal. and Mach. Intell. **13** (1991) 376–380
8. Fitzpatrick, J., West, J., Maurer, C.: Predicting error in rigid-body point-based registration. IEEE Trans. on Medical Imaging **17** (1998) 694–702